Determining doping efficiency and mobility from conductivity and Seebeck data of n-doped C_{60} layers

Torben Menke, Debdutta Ray,* Hans Kleemann, Karl Leo,† and Moritz Riede‡

Institut für Angewandte Photophysik, Technische Universität Dresden, 01062 Dresden, Germany, http://www.iapp.de

(Dated: June 11, 2018)

In this work, we introduce models for deriving lower limits for the key parameters doping efficiency, charge carrier concentration, and charge carrier mobility from conductivity data of doped organic semiconductors. The models are applied to data of thin layers of Fullerene C_{60} n-doped by four different n-dopants. Combining these findings with thermoelectric Seebeck data, the energetic position of the transport level can be narrowed down and trends for the absolute values are derived.

I. INTRODUCTION

The success of inorganic semiconductor devices relies to a large extend on the possibility to control the electrical conductivity and the position of the Fermi level within the semiconductor by electrochemical doping. Also in case of organic semiconductors, doping brings additional benefit to the device, making organic light-emitting diodes (OLEDs), organic photovolataic cells (OPV), and organic field-effect transistors (OFETs) more efficient and reliable.[1–3] Similar to inorganic semiconductors, doping can be achieved for organic semiconductors by deploying either electron donating (n-type) or accepting (p-type) compounds (atoms or molecules).[4, 5] However, while doping in inorganic materials can be sufficiently described within the picture of one transport level and Fermi-Dirac statistics, the complexity of the description of doping in organic semiconductors is caused by their structural and energetical disorder.[6–9] In particular, a self-consistent picture describing the complex interplay between the occupancy of the spatially and energetically distributed sites, the density dependence of charge carrier mobility and the number of ionized doping states has not been drawn.

The aim of this work is to contribute to this understanding by presenting models for the estimation of key parameters of doped organic semiconductor layers: doping efficiency, free charge carrier concentration and mobility. This work focuses on n-doping of small molecules, but the derived models can be applied to p-doping and polymers as well. First, lower limits for the electron mobility, the charge carrier density, as well as the doping efficiency are derived from conductivity data for n-doped C_{60} samples, comparing four different dopants. Second, combining these findings with thermoelectric Seebeck data, the energetic position of the transport level can be narrowed down. Finally, absolute values for the
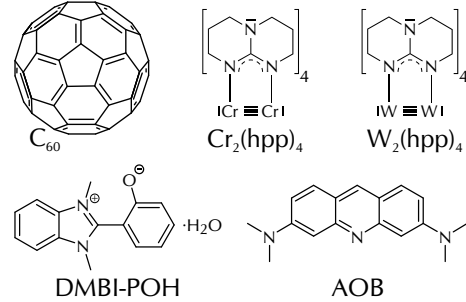
* Now at Department of Electrical Engineering, I.I.T. Madras, Chennai 600036, India

† leo@iapp.de

‡ Now at Physics Department, University of Oxford, Clarendon Laboratory, Parks Road, Oxford OX1 3PU, England, United Kingdom

FIG. 1. Chemical structures of the investigated materials.

key parameters are derived, assuming a constant transport level.

II. MATERIALS AND METHODS

The prominent electron transporting material C_{60} is studied, comparing four n-dopants: tetrakis(1,3,4,6,7,8-hexahydro-2H-pyrimido[1,2-a]pyrimidinato)dichromium (II) and -ditungsten (II) ($Cr_2(hpp)_4$ [10] and $W_2(hpp)_4$ [10]), 3,6-bis(dimethylamino)acridine (AOB [11]), and 2-(1,3-dimethyl-1H-benzoimidazol-3-ium-2-yl)phenolatehydrate (DMBI-POH [11]). The corresponding chemical structures are shown in FIG. 1. $Cr_2(hpp)_4$ and $W_2(hpp)_4$ are rather heavy compounds with low ionization energy and hence reactive with air. AOB and DMBI-POH are more light-weight, air-stable precursor compounds that form their active dopant compound during thermal co-deposition with C_{60} [11, 12]. The measurement data have been published earlier[10, 11, 13], where details concerning sample fabrication and measurement techniques are given. In this work, the data are re-evaluated to derive models and trends for the key parameters of doped layers, while comparing different dopants.

In the following, the doping concentration C is expressed in terms of molar ratio MR being the ratio of the number densities n of dopant (D) to host (H) molecules:

$$C = \frac{n_D}{n_H} \qquad (1)$$

The sum of host and dopant number densities gives the

total number density of molecules n_{Mol}

$$n_{\mathrm{Mol}} = n_{\mathrm{H}} + n_{\mathrm{D}} \; . \tag{2}$$

From equations (1) and (2) follows

$$n_{\mathrm{D}} = n_{\mathrm{Mol}} \cdot \frac{C}{1+C} \; . \tag{3}$$

In an intrinsic layer, n_{Mol} can be derived from the material's mass density ρ and molar mass M, together with Avogadro's constant N_{Avo}:

$$n_{\mathrm{Mol}} = \frac{N_{\mathrm{Avo}} \cdot \rho}{M} \; . \tag{4}$$

For C_{60} the values $\rho = 1.63$ g/cm^3 and $M = 720.6$ g/mol yield a molecular density of $n_{\mathrm{Mol,C_{60}}} = 1.36 \cdot 10^{21}$ cm^{-3}. In the following, the common assumption is made that each dopant molecule substitutes one host molecule and hence n_{Mol} is unaltered upon doping.

The electrical conductivity σ of an n-doped semiconductor can be expressed as the product of density of free electrons n_{e} and the electron mobility μ

$$\sigma = e \cdot n_{\mathrm{e}} \cdot \mu \; , \tag{5}$$

with the elementary charge e. In doped layers, n_{e} is proportional to the number density of dopant molecules n_{D} and the doping efficiency η_{dop} (neglecting the much lower intrinsic charge carrier and trap densities[14])

$$n_{\mathrm{e}} = \eta_{\mathrm{dop}} \cdot n_{\mathrm{D}} \; . \tag{6}$$

Inserting equation (3) into (6) and using (5), n_{e} can be correlated to μ for a measured conductivity σ as

$$\mu = \frac{\sigma}{e \cdot \eta_{\mathrm{dop}} \cdot n_{\mathrm{Mol}}} \cdot \frac{1+C}{C} \; . \tag{7}$$

Both, μ and η_{dop}, are expected to vary with doping concentration.

III. RESULTS

A. Measurement data

Conductivity and thermoelectric Seebeck data, shown in FIG. 2, allow for direct comparison of different n-doped C_{60} systems (20 to 30 nm layer thickness). Data are measured in vacuum at $T = 40\,^\circ$C, after a thermal annealing step at $100\,^\circ$C that ensures reproducibility, as discussed in detail in the original publications. Since all samples showed a linear and symmetric current–voltage dependency, contact resistances are neglected and ohmic injection is assumed.
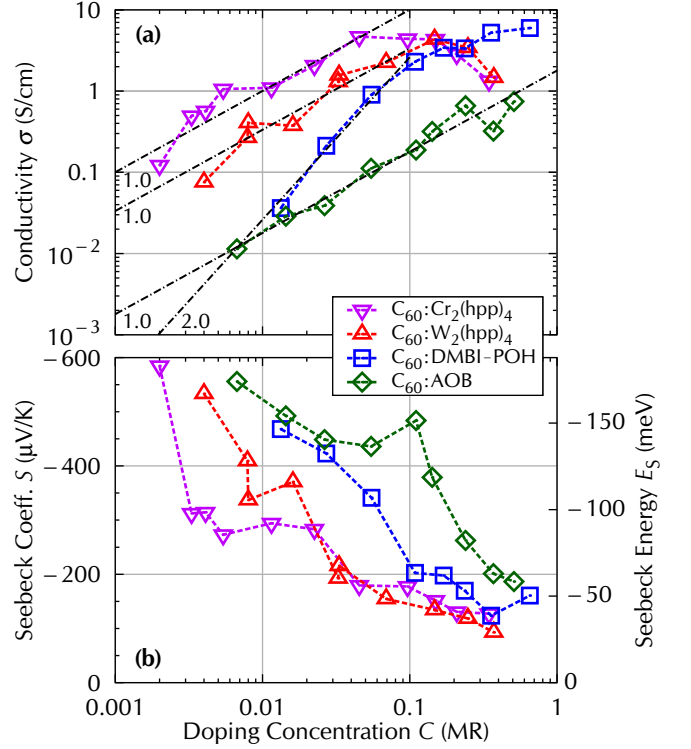

FIG. 2. Measurement data probed in vacuum at $T = 40\,^\circ$C (after thermal annealing) of 20 to 30 nm thin C_{60} layers n-doped by air-stable (AOB and DMBI-POH) and air-sensitive ($Cr_2(hpp)_4$ and $W_2(hpp)_4$) dopants, combined from refs [10, 11, 13]. (a) Conductivity σ and (b) Seebeck coefficient S and Seebeck energy E_S vs. doping concentration C. The chain-dotted lines of slopes 1.0 and 2.0 are guides to the eye.

B. Lower limit of the mobility

According to equation (7), μ is inversely proportional to η_{dop} for a given (measured) conductivity. Consequently, assuming a perfect doping efficiency of $\eta_{\mathrm{dop}} = 100\,\%$ as upper limit (i.e. each dopant molecule is ionized and provides one free charge carrier) a lower limit for the mobility μ_{LL} can be derived from conductivity data at a given doping concentration:

$$\mu_{\mathrm{LL}} = \frac{\sigma}{e \cdot 100\,\% \cdot n_{\mathrm{Mol}}} \cdot \frac{1+C}{C} \; . \tag{8}$$

As in general the real η_{dop} is below $100\,\%$, the real mobility μ must be higher than μ_{LL} to fulfill equation (7). Recently, it has been shown[15] that by using dimer molecules as dopants, two free electrons can be generated per dopant molecule. However, for the dopants used here such behavior is unlikely.

In FIG. 3, this calculation is performed using the n-doped C_{60} conductivity data from FIG. 2 (a), probed at $T = 40\,^\circ$C. μ_{LL} is found to be highest for the dopant $Cr_2(hpp)_4$ with a maximum of $\mu_{\mathrm{LL}} = 0.9$ cm^2/Vs at $C = 0.005$ MR. This value is close to the record mobility reported for undoped C_{60} layers of $\mu = 4.9$ cm^2/Vs[16],
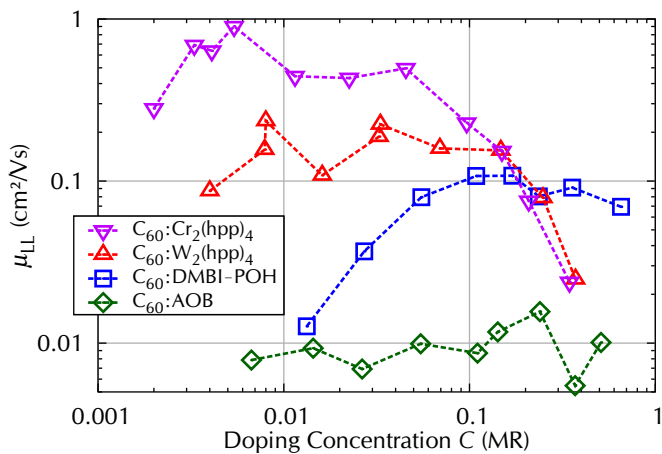
FIG. 3. Lower limit of the electron mobility μ_{LL} for n-doped C_{60}, calculated by equation (8) using the conductivity data from FIG. 2 (a), probed at $T = 40\,^{\circ}$C.

which is measured in an OFET geometry and thus at high n_{e}. At doping concentrations of $C < 0.045$ MR, μ_{LL} is rather constant for $Cr_2(hpp)_4$ with values in the range of $\mu_{\mathrm{LL}} = 0.5$ cm^2/Vs, whereas at higher C the μ_{LL} drops significantly. A similar trend is found for the second air-sensitive dopant $W_2(hpp)_4$. At $C < 0.150$ MR, almost constant values in the range of $\mu_{\mathrm{LL}} = 0.15$ cm^2/Vs are derived, followed by a drop for higher doping concentrations. The reduction of the μ_{LL} suggest that the high density of the large and heavy dopants in the layer leads to a hindering of the transport and hence a reduction of the mobility, as discussed in ref.[10] and supported by OFET studies on n-doped C_{60} layers[17].

A different relation is found for the more light-weight air-stable dopants AOB and DMBI-POH. The samples doped by AOB yield an almost constant value in the order of only $\mu_{\mathrm{LL}} = 9 \cdot 10^{-3}$ cm^2/Vs. Samples doped by DMBI-POH start for low C at a similar value to AOB, but show a strong increase with C. A saturation around $\mu_{\mathrm{LL}} = 0.1$ cm^2/Vs is observed, being even higher than for the air-sensitive dopants at these doping concentrations.

It is expected that for low doping concentrations of each dopant the real values of the electron mobility are the same. Therefore, the different values of the μ_{LL} indicate different doping efficiencies of the dopants, which is addressed in the next section. From this model it cannot be distinguished whether the observed decrease of μ_{LL} at high C for $Cr_2(hpp)_4$ and $W_2(hpp)_4$ is correlated to trends of the real mobility μ or a decreasing η_{dop}.

C. Lower limit of the charge carrier density and the doping efficiency

Apart from estimations for the lower limit of the mobility by assuming $\eta_{\mathrm{dop}} = 100\,\%$, the opposite approach can be performed by knowledge of an upper limit for the mobility μ_{UL}. Such an μ_{UL} allows for deriving a lower
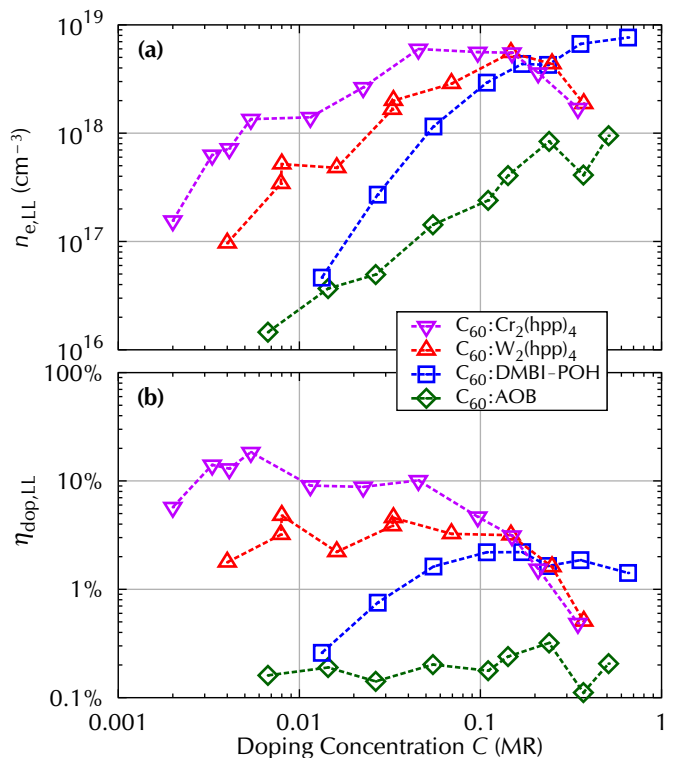

FIG. 4. Lower limits of (a) density of free electrons $n_{\mathrm{e,LL}}$ and (b) doping efficiency $\eta_{\mathrm{dop,LL}}$ for n-doped C_{60}, calculated by assuming a constant mobility, set to the record value for intrinsic C_{60} of $\mu = 4.9$ cm^2/Vs[16] and using the conductivity data from FIG. 2 (a), probed at $T = 40\,^{\circ}$C.

limit of the density of free electrons $n_{\mathrm{e,LL}}$ and doping efficiency $\eta_{\mathrm{dop,LL}}$ via equations (5) and (7)

$$n_{\mathrm{e,LL}} = \frac{\sigma}{e \cdot \mu_{\mathrm{UL}}} \qquad (9)$$

$$\eta_{\mathrm{dop,LL}} = \frac{\sigma}{e \cdot \mu_{\mathrm{UL}} \cdot n_{\mathrm{Mol}}} \cdot \frac{1+C}{C} . \qquad (10)$$

As the real mobility in the used sample geometry is expected to be lower than this upper limit μ_{UL} and furthermore to be negatively affected by the introduction of dopant molecules hindering the transport, the real values of n_{e} and η_{dop} must be larger than $n_{\mathrm{e,LL}}$ and $\eta_{\mathrm{dop,LL}}$ to fulfill equation (7).

The highest reported electron mobility in C_{60} is $\mu = 4.9$ cm^2/Vs[16], measured in an OFET geometry. The free charge carriers in OFETs are generated by the electric field induced by the gate voltage and their number is typically much larger than values achieved by doping.[18] As the mobility of an organic semiconductor usually increases with charge carrier density[19], OFET channel mobilities are generally larger than the mobilities in the bulk material and hence in the conductivity geometry. Therefore, this value can be interpreted as an upper limit μ_{UL}.

The derived $n_{\mathrm{e,LL}}$ values are depicted in FIG. 4 (a), calculated from the conductivity data shown in FIG. 2 (a).

All material combinations show an increase of $n_{\mathrm{e,LL}}$ with doping concentration. The highest $n_{\mathrm{e,LL}}$ close to 10^{19} cm^{-3} are obtained for C$_{60}$ highly doped by DMBI-POH, Cr$_2$(hpp)$_4$ or W$_2$(hpp)$_4$, whereas for AOB the largest value is one order of magnitude lower. These values have to be considered in relation to the total density of molecules of $n_{\mathrm{Mol,C_{60}}} = 1.36 \cdot 10^{21}$ cm^{-3}. For high concentrations of Cr$_2$(hpp)$_4$ and W$_2$(hpp)$_4$ a saturation and decrease in $n_{\mathrm{e,LL}}$ is observed. It might possible that this is an artificial trend, produced by the assumption of a constant mobility. If the real values for n_{e} follow this trend, it is most probably originated in agglomeration and thus shielding of dopants.

In addition to $n_{\mathrm{e,LL}}$, the lower limit of the doping efficiency $\eta_{\mathrm{dop,LL}}$ for each sample is calculated using equation (10) and the results are presented in FIG. 4 (b). As mobility and doping efficiency are inversely proportional, the trends of the curves for $\eta_{\mathrm{dop,LL}}$ correspond to the trends of the lower limits of the mobilities μ_{LL}, presented in FIG. 3. C$_{60}$ doped by Cr$_2$(hpp)$_4$ leads to a maximum value of $\eta_{\mathrm{dop,LL}} = 18\,\%$ at $C = 0.005$ MR and an almost constant $\eta_{\mathrm{dop,LL}} \approx 10\,\%$ up to $C = 0.045$ MR, followed by a decrease for the highest doping ratios used. Samples comprising W$_2$(hpp)$_4$ yield efficiencies around $\eta_{\mathrm{dop,LL}} = 3\,\%$ and a drop at $C > 0.150$ MR. AOB-doped samples have the lowest values of around $\eta_{\mathrm{dop,LL}} = 0.2\,\%$. DMBI-POH samples start at a similar value, but rise 10-fold to a saturation around $\eta_{\mathrm{dop,LL}} = 2\,\%$ at high doping concentrations. The gain in $\eta_{\mathrm{dop,LL}}$ for low C of DMBI-POH samples is most probably correlated to an increasing real η_{dop} in this range, as it is unlikely that only for one dopant the mobility of C$_{60}$ is rising with the doping concentration.

At low doping concentrations, the real mobilities are expected to be least affected by the dopants and are consequently similar for all four material combinations. Therefore, the calculated $\eta_{\mathrm{dop,LL}}$ at low C can be directly compared and is expected to be correlated to the real doping efficiency η_{dop} by a constant factor. This factor is given by the ratio of the used upper limit of the mobility $\mu_{\mathrm{UL}} = 4.9$ cm^2/Vs and the real value of the bulk material in this sample geometry. Hence, at low doping concentration, the real doping efficiency η_{dop} of Cr$_2$(hpp)$_4$ is approximately 3 times higher than for W$_2$(hpp)$_4$ and around 15 times higher than for AOB and DMBI-POH. Consequently, for low C of these two dopants an upper limit $\eta_{\mathrm{dopUL}} = 100\,\% \div 15 = 6.7\,\%$ is derived.

D. Conclusions from Seebeck measurements

The density of free electrons n_{e} is furthermore given by the integral of the product of the density of states $DOS(E)$ and the Fermi-Dirac distribution function $f_{\mathrm{FD}}(E, E_{\mathrm{F}})$ over all energies:

$$n_{\mathrm{e}} = \int_{-\infty}^{\infty} DOS(E) \cdot f_{\mathrm{FD}}(E, E_{\mathrm{F}}) \, dE \ . \qquad (11)$$
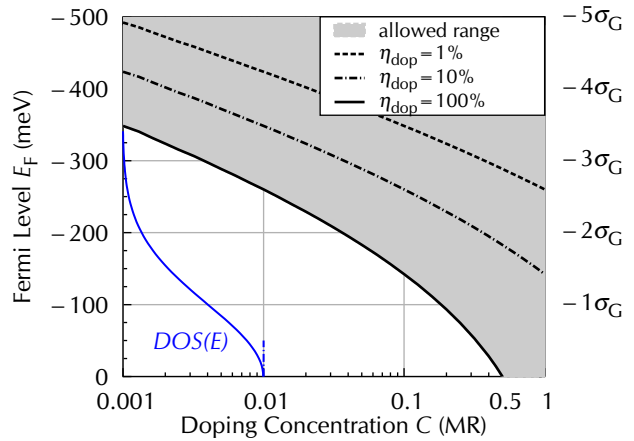

FIG. 5. Calculated Fermi level position $E_{\mathrm{F}}(C)$ with respect to the maximum of the Gaussian density of states for different doping efficiencies η_{dop}. Derived using equation (12) and a Gaussian DOS with $\sigma_{\mathrm{G}} = 100$ meV and $T = 40\,^{\circ}$C. Only values in the gray area are physically allowed with $\eta_{\mathrm{dop}} \leq 100\,\%$.

Thus, for a known $DOS(E)$ and given η_{dop}, the position of the Fermi level E_{F} can be derived via comparing the n_{e} values with equation (6). Using a Gaussian density of states for modeling the energetic disorder of C$_{60}$ and setting its maximum to the position at $E = 0$, it follows:

$$n_{\mathrm{e}} = \eta_{\mathrm{dop}} \cdot n_{\mathrm{D}} \qquad (6)$$

$$= \int_{-\infty}^{\infty} \frac{n_{\mathrm{H}}}{\sqrt{2\pi}\,\sigma_{\mathrm{G}}} \exp\left(-\frac{E^2}{2\sigma_{\mathrm{G}}^2}\right) \cdot \frac{1}{1 + \exp\left(\frac{E - E_{\mathrm{F}}}{k_{\mathrm{B}} T}\right)} \, dE \ . \qquad (12)$$

Again, n_{D} and n_{H} are related to C via equations (1) and (3). σ_{G} is the standard deviation of the distribution. In the following, a constant value of $\sigma_{\mathrm{G}} = 100$ meV for all C is assumed, which is chosen to be somewhat higher than the reported $\sigma_{\mathrm{G}} = 88$ meV[20] for undoped C$_{60}$, to compensate the influence of doping that might broaden the DOS [14]. The inversion of equation (12) to obtain E_{F} as function of C and η_{dop} is performed numerically and the results are plotted in FIG. 5. The solid line represents the E_{F} at $\eta_{\mathrm{dop}} = 100\,\%$. As the doping efficiency cannot exceed $100\,\%$, only values above this line are physically allowed. It can be seen that with increasing C, E_{F} reaches densely populated regions of the DOS, when assuming a constant η_{dop}.

This approach is now combined with data from Seebeck studies, to calculate the position of the transport level E_{Tr}, with respect to the maximum of the DOS. E_{Tr} is defined as the energy weighted by the differential conductivity $\sigma'(E)$[21]

$$E_{\mathrm{Tr}} = \frac{1}{\sigma} \int_{-\infty}^{+\infty} E\,\sigma'(E) \, dE \ . \qquad (13)$$

The measured Seebeck coefficient S (at a certain doping concentration) is directly proportional to the ener-
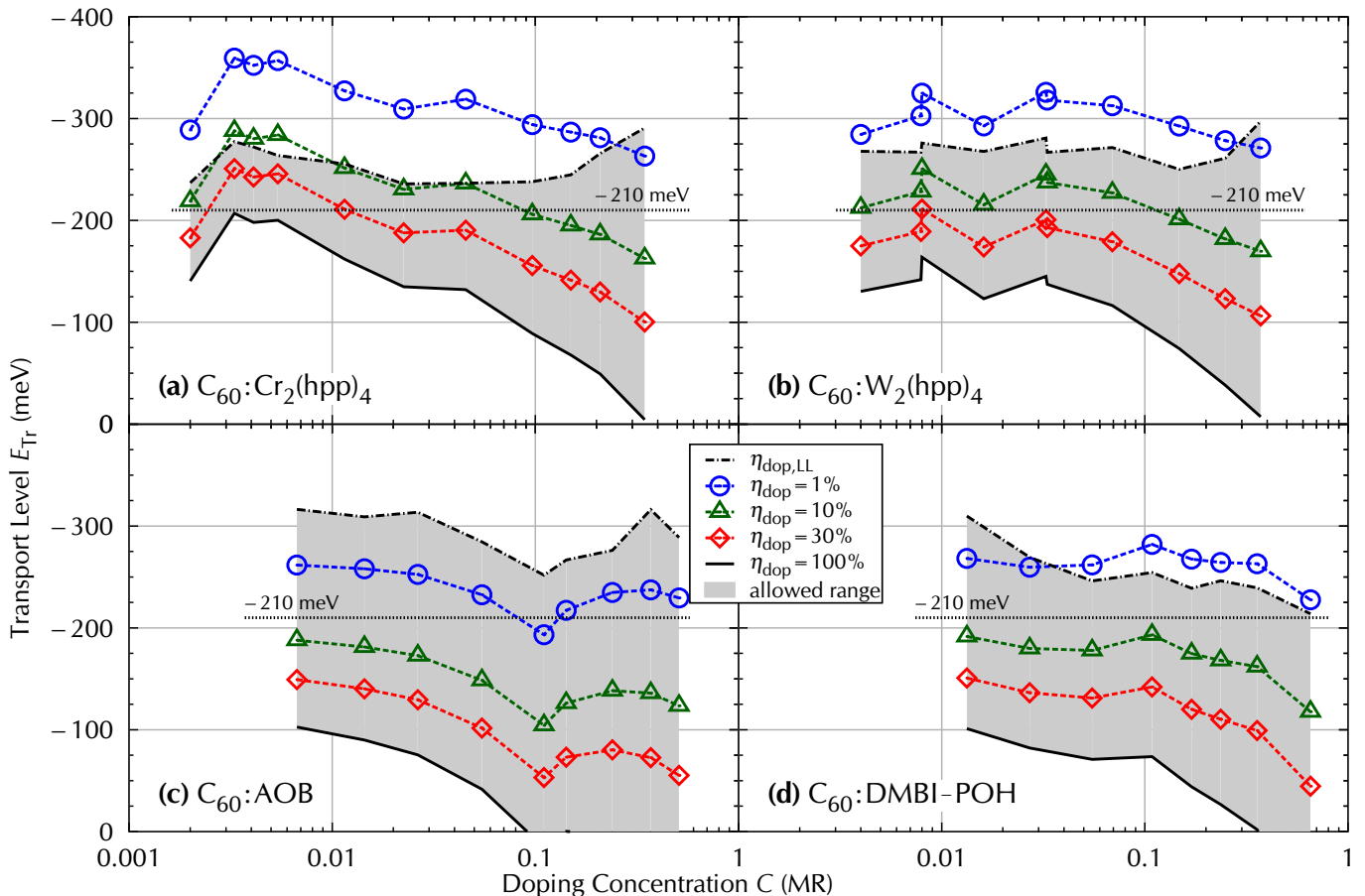
FIG. 6. Calculated transport level position E_{Tr} with respect to the maximum of the Gaussian density of states for varying doping concentration and doping efficiency η_{dop}. Obtained by subtracting measured E_S (FIG. 2 (b)) from calculated $E_F(C)$ (FIG. 5). Parameters used: $\sigma_G = 100$ meV and $T = 40\,°C$. The gray area corresponds to the physically allowed range between lower and upper limit of the doping efficiency. The dashed line at $E_{Tr} = -210$ meV indicates a value that is allowed for all samples.

getic difference between Fermi level and transport level [21, 22], denoted as E_S in the following. Subtracting this measured E_S from E_F, the position of $E_{Tr} = E_F - E_S$ can be derived. Again, E_F is calculated as discussed above for a given η_{dop} and varying C. This calculation is performed for several different values of η_{dop}, and the results are shown in FIG. 6. As the doping efficiency must be be greater than the above derived lower limit $\eta_{dop,LL}$ and cannot exceed $\eta_{dop} = 100\,\%$, only a certain region of E_{Tr} is consistent with all data, marked by the gray shaded areas in FIG. 6. This physically possible region is for most samples between $E_{Tr} = -300$ meV and -100 meV with respect to the maximum of the Gaussian density of states. It is narrowest for $Cr_2(hpp)_4$, due to the large value obtained for $\eta_{dop,LL}$.

E. Assuming a constant transport level

The narrow region of allowed E_{Tr} values suggests the assumption of a constant transport level for all samples

and doping concentrations as a further approximation. This allows for deriving values and general trends from the data. A value of $E_{Tr} = -210$ meV is chosen, as this value is in the allowed regime for all samples, indicated by the dotted line in FIG. 6.

Analogue to FIG. 5, trends for $E_S(C, \eta_{dop})$ can be derived by subtracting this $E_{Tr} = -210$ meV from calculated $E_F(C)$, shown as lines in FIG. 7. These trends are now compared to the measured Seebeck data (symbols in FIG. 7). It can be seen that under the assumption of a fixed E_{Tr}, the Seebeck results of C_{60} doped by $C < 0.100$ MR of $W_2(hpp)_4$ or DMBI-POH follow the trend of a constant doping efficiency, whereas at larger C the E_S tends towards lower η_{dop}. The samples doped by $Cr_2(hpp)_4$ and AOB show deviations from the tendency of a constant η_{dop}.

Using this fixed $E_{Tr} = -210$ meV, the corresponding density of free electrons n_e is calculated for each sample by solving the integral (12) of the product of DOS and Fermi distribution f_{FD}. Here, the measured E_S is used to calculate the Fermi level position $E_F = E_{Tr} + E_S$. The
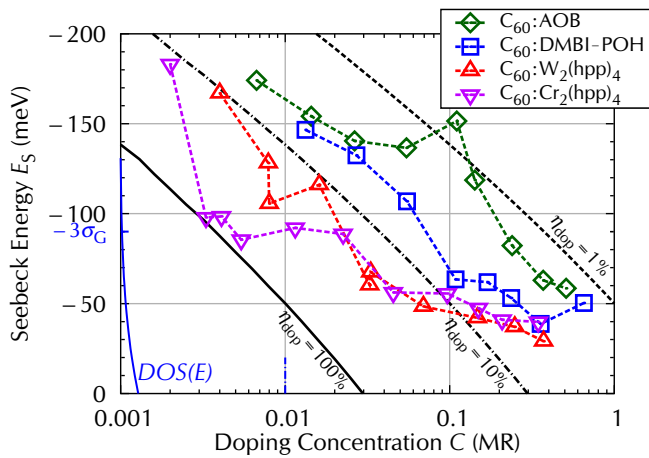
FIG. 7. Measured Seebeck energy E_S ($T = 40\,°\text{C}$) compared to calculated $E_S(C)$ for constant transport level $E_{\text{Tr}} = -210\,\text{meV}$ at different doping efficiencies η_{dop}. Calculations performed analogously to FIG. 5 and subtracting E_{Tr}. Only values above the solid black line corresponding to $\eta_{\text{dop}} = 100\,\%$ are physically allowed. The *DOS* is sketched by the blue line using the same scale as in FIG. 5. The Fermi level position E_F is given by the sum of E_S and E_{Tr}.

results are shown in FIG. 8 (a).

For all four material combinations, the calculated n_e increases with C until at high C a saturation is observed. Samples doped by $\text{Cr}_2(\text{hpp})_4$ or $\text{W}_2(\text{hpp})_4$ saturate around $n_e = 10^{19}\,\text{cm}^{-3}$ for doping concentrations $C \geq 0.040\,\text{MR}$. The same n_e is reached by DMBI-POH samples, but at higher C. AOB-doped samples saturate around lower $n_e = 5 \cdot 10^{18}\,\text{cm}^{-3}$ for $C > 0.100\,\text{MR}$. These values have again to be seen in relation to the density of molecules of $n_{\text{Mol,C}_{60}} = 1.36 \cdot 10^{21}\,\text{cm}^{-3}$. Overall, these trends seem to be more realistic than those derived under the assumption of constant mobility, compare FIG. 4 (a), where a decrease of the lower limit of the density of free electrons $n_{e,\text{LL}}$ is found at high doping concentrations of $\text{Cr}_2(\text{hpp})_4$ and $\text{W}_2(\text{hpp})_4$.

The doping efficiency η_{dop} can be derived from known n_e, as shown in FIG. 8 (b). A maximum of $\eta_{\text{dop}} = 92\,\%$ is found for the sample of $C = 0.0033\,\text{MR}$ of $\text{Cr}_2(\text{hpp})_4$, showing that lower values than $E_{\text{Tr}} = 210\,\text{meV}$ are not realistic, as these would result in an even larger value of η_{dop}, which cannot exceed $100\,\%$. Larger values of E_{Tr} on the other hand would lead to a violation of the lower limit of $\eta_{\text{dop,LL}}$, as derived in section III C. Hence, only values around $E_{\text{Tr}} = -210\,\text{meV}$ are compatible with all measurements. The doping efficiencies of $\text{Cr}_2(\text{hpp})_4$ and $\text{W}_2(\text{hpp})_4$ samples decrease with doping concentration and both series are in excellent agreement for $C \geq 0.040\,\text{MR}$. AOB-doped samples show a similar trend but at lower values, whereas for DMBI-POH an almost η_{dop} is observed.

The mobility μ can be calculated from equation (5) by combining the derived values of the density of free electrons n_e and the measured conductivity data. The
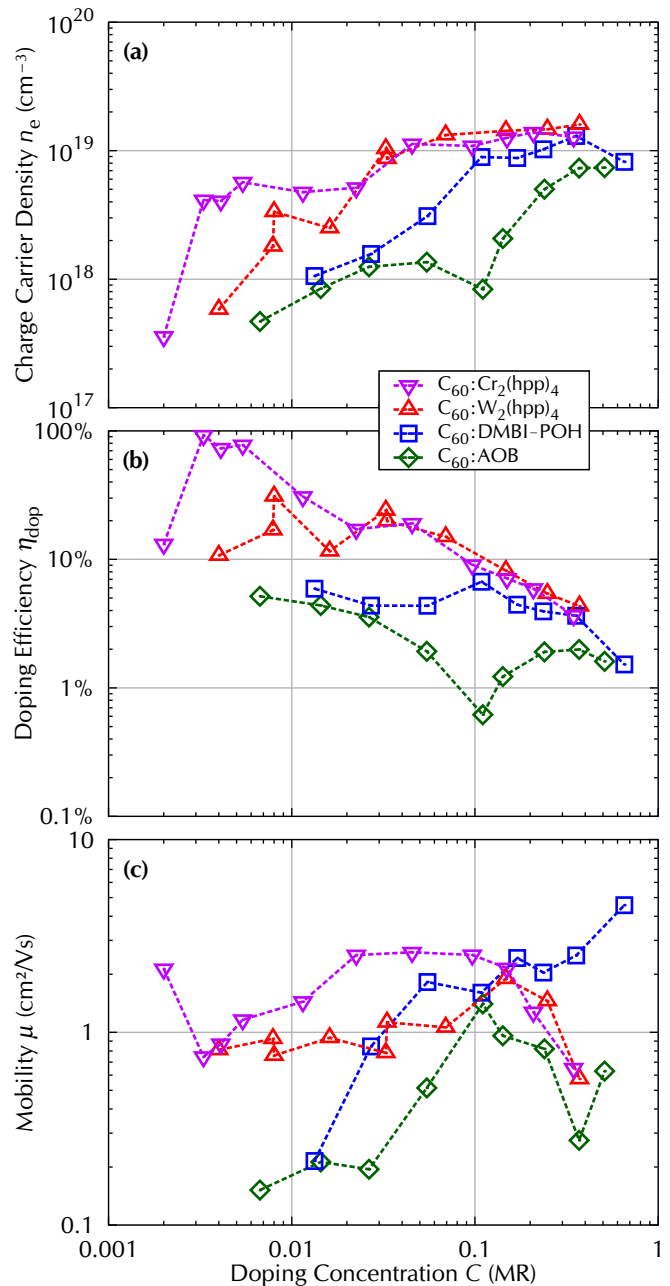

FIG. 8. Calculated values of (a) charge carrier density n_e, (b) doping efficiency η_{dop} and (c) mobility μ for n-doped C_{60}. Based on the assumption of a constant transport level $E_{\text{Tr}} = -210\,\text{meV}$, using $\sigma_G = 100\,\text{meV}$ and measured conductivity and Seebeck data shown in FIG. 2.

results are presented in FIG. 8 (c). Rather high values are found, in agreement with the μ_{LL}, derived in section III B. Both, $\text{Cr}_2(\text{hpp})_4$ and $\text{W}_2(\text{hpp})_4$, yield an almost constant mobility at low and medium C, followed by a decrease at high C that might be attributed to changes in the morphology as discussed in ref.[10]. Most of the mobilities derived for $\text{W}_2(\text{hpp})_4$ samples are lower than those for $\text{Cr}_2(\text{hpp})_4$. This effect can be interpreted as doping by $\text{W}_2(\text{hpp})_4$ resulting into a reduc-

tion of the electron mobility, which might originate from its extremely small ionization energy IE = 2.68(13) eV (compared to 3.95(13) eV for $Cr_2(hpp)_4$)[10] and thus strong tendency towards ionization. The samples doped by AOB or DMBI-POH show low mobilities at low C and an increase in the medium doping regime. For AOB-doped samples, a decrease at high C is observed, whereas for DMBI-POH the mobility rises further, up to a value of $\mu = 4.6$ cm^2/Vs, close to the expected limit of $\mu_{UL} = 4.9$ cm^2/Vs.

Overall, the results derived on the basis of the assumption of a constant transport level E_{Tr} for all samples seem reasonable, as both, the values and the trends are in the expected range. In general, it is expected that E_{Tr}, which is defined as the energy weighted by the differential conductivity $\sigma'(E)$ (compare equation (13)) shifts upon increasing doping concentration towards the maximum of the Gaussian density of states (and hence to lower values), as the maximum of $\sigma'(E)$ is expected to shift in this direction. This would result in an upward shift of the trend of n_e and thus η_{dop} with C, whereas the mobility would be shifted downwards. Modeling this would require detailed knowledge on the energetic distribution of the mobility $\mu(E)$ contributing to $\sigma'(E)$[21].

IV. CONCLUSION

The simple models presented in the first part are powerful tools for deriving lower limits of the important parameters charge carrier mobility, density of free electrons and doping efficiency from conductivity data of doped layers. These give an insight to the trends of the corresponding real values and allow to compare the relative values for different material combinations. The methods can easily be adopted for p-doped samples[13, 23] as well as for polymers.

Even without knowledge of the energetic dependency of the macroscopic mobility $\mu(E)$, it is shown that by combining Seebeck and conductivity studies, it is possible to narrow down the physically allowed regime for the transport level.

The assumption of a constant transport level position for all samples yields reasonable trends for density of free electrons, doping efficiency and mobility. A more sophisticated model would require profound knowledge of the shape of the density of states and the energetic distribution of the mobility, as well as of the influence of doping on these, which are pathways for future studies.

[1] S. Reineke, F. Lindner, G. Schwartz, N. Seidler, K. Walzer, B. Lüssem, and K. Leo, Nature **459**, 234 (2009).

[2] M. Riede, C. Uhrich, J. Widmer, R. Timmreck, D. Wynands, G. Schwartz, W.-M. Gnehr, D. Hildebrandt, A. Weiss, J. Hwang, S. Sundarraj, P. Erk, M. Pfeiffer, and K. Leo, Advanced Functional Materials **21**, 3019 (2011).

[3] F. Ante, D. Kälblein, U. Zschieschang, T. W. Canzler, A. Werner, K. Takimiya, M. Ikeda, T. Sekitani, T. Someya, and H. Klauk, Small **7**, 1186 (2011).

[4] K. Walzer, B. Männig, M. Pfeiffer, and K. Leo, Chemical Reviews **107**, 1233 (2007).

[5] B. Lüssem, M. Riede, and K. Leo, Physica Status Solidi A **210**, 9 (2013).

[6] B. A. Gregg, S.-G. Chen, and R. A. Cormier, Chemistry of Materials **16**, 4586 (2004).

[7] V. Arkhipov, P. Heremans, E. Emelianova, and H. Bässler, Physical Review B **71**, 045214 (2005).

[8] A. Mityashin, Y. Olivier, T. Van Regemorter, C. Rolin, S. Verlaak, N. G. Martinelli, D. Beljonne, J. Cornil, J. Genoe, and P. Heremans, Advanced Materials **24**, 1535 (2012).

[9] I. Salzmann, G. Heimel, S. Duhm, M. Oehzelt, P. Pingel, B. George, A. Schnegg, K. Lips, R.-P. Blum, A. Vollmer, and N. Koch, Physical Review Letters **108**, 035502 (2012).

[10] T. Menke, D. Ray, J. Meiss, K. Leo, and M. Riede, Applied Physics Letters **100**, 093304 (2012).

[11] T. Menke, P. Wei, D. Ray, H. Kleemann, B. D. Naab, Z. Bao, K. Leo, and M. Riede, Organic Electronics **13**, 3319 (2012).

[12] B. D. Naab, S. Guo, S. Olthof, E. G. B. Evans, P. Wei, G. L. Millhauser, A. Kahn, S. Barlow, S. R. Marder, and Z. Bao, Journal of the American Chemical Society **135**, 15018 (2013).

[13] T. Menke, *Molecular Doping of Organic Semiconductors – A Conductivity and Seebeck Study*, Dissertation, TU Dresden, ISBN 978-3-8439-1177-1, (2013).

[14] P. Pahner, H. Kleemann, L. Burtone, M. L. Tietze, J. Fischer, K. Leo, and B. Lüssem, Physical Review B **88**, 195205 (2013).

[15] S. Olthof, S. Mehraeen, S. K. Mohapatra, S. Barlow, V. Coropceanu, J.-L. Brédas, S. R. Marder, and A. Kahn, Physical Review Letters **109**, 176601 (2012).

[16] K. Itaka, M. Yamashiro, J. Yamaguchi, M. Haemori, S. Yaginuma, Y. Matsumoto, M. Kondo, and H. Koinuma, Advanced Materials **18**, 1713 (2006).

[17] K. Harada, F. Li, B. Männig, M. Pfeiffer, and K. Leo, Applied Physics Letters **91**, 92118 (2007).

[18] L. G. Kaake, P. F. Barbara, and X.-Y. Zhu, The Journal of Physical Chemistry Letters **1**, 628 (2010).

[19] W. F. Pasveer, P. a. Bobbert, and M. a. J. Michels, Physica Status Solidi C **1**, 164 (2004).

[20] I. I. Fishchuk, A. K. Kadashchuk, J. Genoe, M. Ullah, H. Sitter, T. B. Singh, N. S. Sariciftci, and H. Bässler, Physical Review B **81**, 045202 (2010).

[21] R. Schmechel, Journal of Applied Physics **93**, 4653 (2003).

[22] H. Fritzsche, Solid State Communications **9**, 1813 (1971).

[23] T. Menke, D. Ray, H. Kleemann, M. P. Hein, K. Leo, and M. Riede, Organic Electronics **15**, 365 (2014).